PROJECT I.2
PLASMA ENABLED NANOFABRICATION:
PROCESSING, SIMULATION, METROLOGY AND APPLICATIONS

Key Researchers: E. Gogolides, A. Tserepi

Permanent Scientific Staff: V. Constantoudis

Post Doctoral Scientists: G. Kokkoris, D. Moschou, N. Vourdas, K. Tsougeni, G. Papadakis

Collaborating Researchers:

- For activity A-Plasma Nanofabrication: I. Raptis (optical characterization), A. Olziersky
  (e-beam lithography)
- For activity D2-Microfluidics-Lab on Chip for Life Sciences: S. Chatzandroulis, K. Misiakos
- For activity D3-Nanodevices for Energy: P. Argitis, P. Normand, P. Dimitrakis, M. Vasilopoulou

PhD Students: M.-E.Vlachopoulou, A. Malainou, D. Kontziampasis, K. Ellinas, A. Smyrnakis, N. Skoro, V.K. Murugesan Kuppuswamy

MSc Students: A. Zeniou, E. Kouris, N. Karasmani, S. Mouchtouris, Th. Christoforidis

External collaborators:

- For activity A-Plasma Nanofabrication: C. Cardinaud (Univ. of Nantes, France), W. Coene, M. Riepen, M. Van Kampen (ASML, Netherlands), D. Ehm (Zeiss, Germany), U. Cvelbar (Josef Stefan Inst., Slovenia), N. Puač, S. Lazovic (Inst. of Physics, Belgrade, Serbia)
- For activity B-Nanometrology: W. Coene (ASML, Netherlands), G. Gallatin (NIST, USA), R. Gronheid, A.P. Vaglio (IMEC, Belgium), E. Pargon (CEA/LETI, France)
- For activity C-Modeling and Simulation: A. Boudouvis, N. Cheimarios, G. Pashos, (NTUA, Greece), C. Vahlas (U.de Toulouse, France), P. Brault, A.L. Thomann (Univ. d'Orléans, France), G. Gallatin (NIST, USA)
- For activity D1-Smart Nanostructured Surfaces: A. Boudouvis, A. Papathanasiou, D.P. Papageorgiou, C. Charitides, E. Pavlatou (NTUA, Greece), K. Beltsios, I. Panagiotopoulos (Univ. of Ioannina, Greece), E. Amanatides, D. Mataras (Univ. of Patras, Greece), H. Zuilhof, S. Pujari (Wageningen Univ., Netherlands)
- For activity D2-Microfluidics-Lab on Chip for Life Sciences: S. Kakabakos, P. Petrou (IRRP, NCSR-D, Greece), A. Vlahou, S. Pagakis (IIBEAA, Greece), G. Kaltsas (TEI of Athens, Greece), D.S. Mathioulakis (NTUA, Greece), E. Sarantopoulou (NHRF, Greece), E. Gizeli (FORTH, Greece), A. Speliotis (IMS, NCSR-D, Greece), T. Rudin, S.E. Pratsinis (ETH Zurich, Switzerland), J.L. Viovy, S. Descroix (Inst. Curie, France), B. Depuis (Inst. Pasteur, Paris, France), G. Jobst (Jobst Technologies, Germany)
- For activity D3-Nanodevices for Energy: S. Christiensen (IMPP, Germany)

OBJECTIVES

The activities of project I.2 can be seen schematically below:

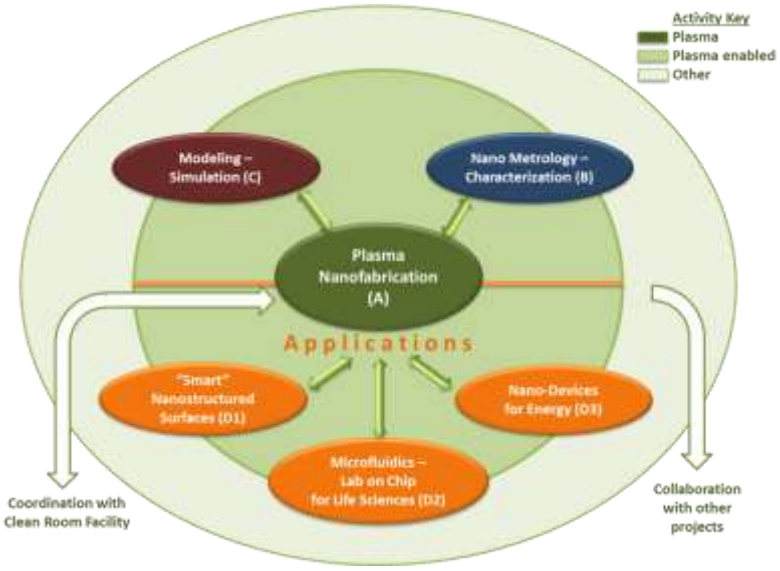

Fig.1. *Schematic of project I.2 activities for Plasma Enabled Nanofabrication*

The heart of our activities and our first objective is to advance and promote plasma nanofabrication, nanopatterning and plasma nanotechnology enabling various applications. This is seen as the central circle in Fig.1 and described in section A below.
Around plasma nanotechnology a series of activities for nanometrology-characterization (B), modeling-simulation (C) and applications (D) are clustered depicted visually in the second circle around A. A third outer circle includes other activities not directly enabled by plasma nanotechnology but linked to the activities of the second circle (B, C, D), as well as to other projects.
Indeed, after fabrication of micro and nanostructures and devices using plasma processing, **our second objective is to develop nanometrology and characterization methodologies for nanostructure description** (see section B). **Our third objective is to understand and improve plasma and other processes using modeling and simulation** (see section C). Finally, **our fourth objective is to exploit our plasma nanotechnology** toolbox to enable **a variety of applications including Surface Engineering** ("smart surfaces" see section D1), **Microfluidics and Lab on Chip for Life Sciences** (see section D2), **and NanoDevices for Energy** (see section D3). For all these objectives, we work in coordination with the clean room facility, often transferring samples to and from it, and in collaboration with several other projects such as the Biomicrosystems project, and the Lithography project.

For 2012 our main achievements are:
Plasma Nanonofabrication: We improved our new planar technology to fabricate, nanotexture (nanoroughen) and surface-modify polymeric microfluidics and bioMEMS (cf. A.1). We established our recent plasma-directed assembly process for nanodot formation on plasma etched polymers (cf. A.2). We characterized Hydrogen Plasmas for plasma cleaning of sensitive optical surfaces (cf. A.3). We developed two novel plasma processes for ultra high aspect ratio fabrication of Silicon Nanowires and nanopillars and measured their optical properties (cf. A.4).
Nanometrology: We developed a methodology to measure the thickness of thin protein and other films on nanostructured surfaces using AFM data (cf. B.1). We developed software for the extraction of noise from SEM images and measurement of Line-Edge-Roughness (cf. B.2). We initiated the use of complex network theory for the description of rough surfaces (cf. B.3).
Modeling and Simulation: We proposed a simple model and rules of thumb for Line-Edge-Roughness Transfer during Plasma Etching (cf. C.1). We modeled Hydrogen Plasmas for Surface Cleaning (cf. C.2). We modeled the lithography process effects on Contact-Edge-Roughness (cf. C.3). We performed Multiscale and molecular Dynamics Simulations for Chemical Vapour Deposition of Si and Al (cf. C.4, C.5). We developed a computational framework for calculation of Cassie-Wenzel transition of drops sitting on microstructured surfaces (cf. C.6).
"Smart" Nanostructured Surfaces: We developed hierarchical superoleophobic surfaces on organic polymers (PMMA, PEEK, PS, PET etc) and on silicones (PDMS) using Oxygen and SF_6 plasma nanotexturing, respectively. New self-assembled fluorinated monolayers were used

for their surface energy reduction. Low hysteresis and high contact angle were obtained for several oils (cf. D1.1, D1.2, D1.3).
Microfluidics and Lab on Chip for Life Sciences: We compared the flow in rough hydrophilic and superhydrophobic microchannels using pressure drop and Particle Image Velocimetry experiments, and showed the reduced pressure drop and large slip velocities in the second case (cf. D2.1, D2.2). We fabricated TiO_2 affinity microcolumns and demonstrated phosphopeptide enrichment (cf. D2.3). We fabricated a DNA amplification Lab on Chip (μPCR) on a polymeric substrate with accurate temperature control (cf. D2.4). We developed new nanoscale arrays of proteins using colloidal lithography followed by plasma etching and selective protein immobilization (cf. D2.5).
Nanodevices for Energy: We established our first Silicon Nanowire p-n junction devices and demonstrated good photovoltaic performance (cf. D3.1).

FUNDING

- SPAM, Marie Curie-ITN,Contract No 215723
- "DNA on waves: an integrated diagnostic system" GSRT Contract No. LS7(276)
- CORSED, Contract No. PE8(844)
- Love Food, Contract No. 317742
- Plasma Nanofactory, Contract No. 695
- DesireDrop, Contract No. MIS 380835
- Project III41011 of MESTD of Serbia and Post Doctoral Fellowship from Serbian Government for Dr Nevena Puac

MAIN RESULTS in 2012

A. Plasma Nanofabrication

A.1 A planar technology for polymeric chip micro-patterning, applicable to microfluidics and labs on chip

K. Tsougeni, E. Gogolides

We propose a new technology for polymeric microchip fabrication based on lithography directly on the polymeric substrate followed by plasma etching of the substrate. We developed lithographic processes for thick and easily strippable photoresist patterning, (where stripping is performed without attacking the polymeric substrate) and plasma etching processes to transfer the pattern and chemically modify the polymeric substrates providing microfluidic channels with desired geometrical and wetting characteristics. We ensured that the photoresist has high resolution for photoresist heights of 5-20 microns (for example resolution down to 1 - 4 μm). In case the photoresist is used to transfer the pattern on the substrate we selected photoresists with high etch resistance and high selectivity with respect to the polymeric substrate. We evaluated single layer, bilayer silicon containing resists, and hard metallic masks. We tested different kinds of photoresists: (a) strippable thick resists such as AZ 15nXT (negative), AZ 9260 (positive), and maP-1275 (positive). However, we noticed deformation of posts after the plasma processing. This process is therefore not suitable for deep polymer etching. (b) Bilayer Si containing strippable photoresist, such as Ormocomp (negative) in combination with a bottom release layer (LOR=Lift-Off-Resist). Lithography is done on the stack LOR layer / Ormocomp. Removal of the LOR can be easily done using weak alkaline solutions, thus the technology is applicable even to extremely sensitive polymeric substrates. Fig.2 shows SEM images of a bilayer of LOR / Ormocomp after O_2 plasma etching before and after removal of the stack. High selectivity (Selectivity 30:1) was obtained after plasma etching because of ORMOCER oxidation to SiO_2. After removing the LOR / ORMOCER stack, clean polymeric surfaces are obtained allowing thermal bonding of the microfluidic lid. We concluded that this resist is a good candidate for patterning and deep etching of polymeric substrates, followed by thermal bonding.

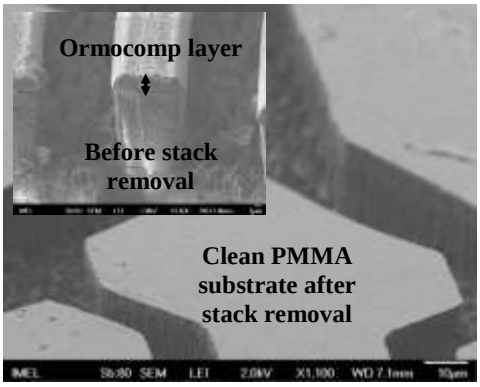

Fig.2. *SEM images of a bilayer of LOR / Ormocomp after O_2 plasma etching before and after removal of the stack.*

A.2 Plasma Directed Organization of Nanodots on Polymers: A statistical analysis as a study on the reproducibility of the phenomenon.

D. Kontziampasis, E. Gogolides

In the previous years, we demonstrated a plasma directed, organized, nanodot formation on organic polymers. This year, we expand our work on plasma directed organization and perform statistics to see how reproducible the phenomenon is, i.e. if it produces the same results using the same reactor, the same plasma etching conditions and the same polymeric material. Also we study whether in the same sample all the areas that are measured have the same statistical characteristics (order, height, width, period etc.) under the same plasma etching conditions, since plasma is considered to be uniform in this area.
The statistical analysis was performed measuring the parameters of samples etched since 2007 and up to 2012. The etching conditions used are; 1 min etching, O_2 plasma, pressure 0.75 Pa, temperature (electrode) 65^{o}C, bias Voltage 0V (Bias generator closed), gas flow 100 sccm and power 1800 W. The statistical parameters measured in this study were the root mean square (rms), correlation length, period and order parameter of the surfaces. The analysis was performed after measuring the samples with AFM (CP-II from Veeco) and analyzing the x-y-z topography of each surface with the home-made software SURFANALYSIS.

Table I. Statistical analysis of 50 different samples, etched under the same conditions for a period of 5 years.

Parameter / Statistics	RMS (nm)	Period λ (nm)	Correlation Length (ξ) (nm)	Order Parameter ω
Mean Value	5.86	62.3	13.9	1.6
Standard Deviation	0.43	7.2	3.2	0.4

Table I shows the size and order parameters after analyzing AFM measurements of surfaces that were etched from 2008 to 2012. A total of 50 different samples were analyzed. In it, we observe a significant deviation in the statistics of the surfaces. Nevertheless, we know that the plasma reactor has undergone through several changes due to maintenance and repairs. The most important one was the maintenance in the cooling system, which can bring significant change in the temperature of the sample during etching. In order to be certain that the deviations are not affected by the changes in the reactor, we perform a series of experiments in which the samples are etched at the same day. Table I shows the analysis of the etched surfaces that were etched the same day (7 samples measured), after AFM measurements. As in the previous series, we calculate rms, correlation length, period and order parameter for each surface.

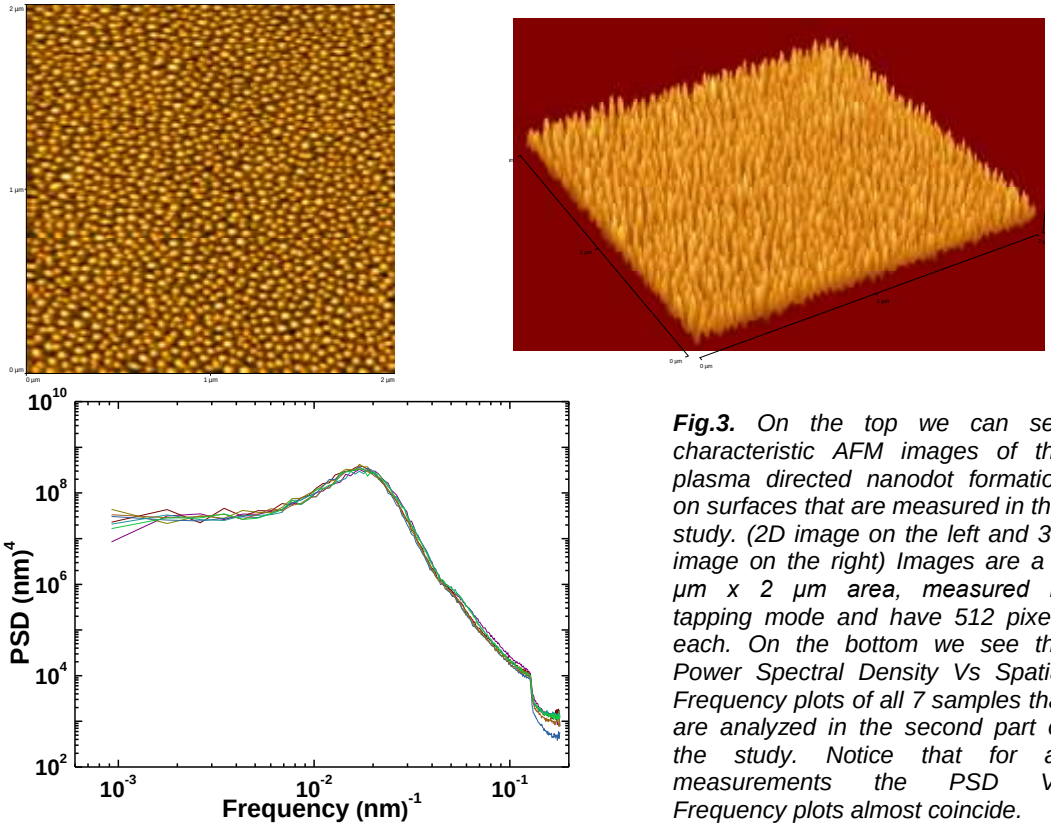

Fig.3. *On the top we can see characteristic AFM images of the plasma directed nanodot formation on surfaces that are measured in this study. (2D image on the left and 3D image on the right) Images are a 2 μm x 2 μm area, measured in tapping mode and have 512 pixels each. On the bottom we see the Power Spectral Density Vs Spatial Frequency plots of all 7 samples that are analyzed in the second part of the study. Notice that for all measurements the PSD Vs Frequency plots almost coincide.*

Table II. Statistical analysis of 7 different samples, etched under the same conditions at the same day.

Parameter / Statistics	RMS (nm)	Period λ (nm)	Correlation Length (ξ) (nm)	Order Parameter ω
Mean Value	**6.16**	**57.9**	**10.6**	**1.8**
Standard Deviation	**0.10**	**1.9**	**1.9**	**0.2**

By observing the values of Table II we can clearly see that the standard deviation is below 10% and lies in the limits of statistical error of each measurement with the AFM.
From the above we can conclude that as long as the reactor's condition is unchanged this method can produce well defined, uniform, nanostructures of the same average height, width, distance and order on the surface of polymeric films.

A.3 Characterization and global modeling of low-pressure Hydrogen-based RF plasmas suitable for surface cleaning processes

N. Škoro, N. Puač, G. Kokkoris, E. Gogolides and external collaborators

We performed measurements and global modeling of low-pressure inductively coupled H_2 plasma which is suitable for surface cleaning applications aiming at understanding mirror cleaning in an Extreme Ultraviolet Lithography (EUVL) Tool. The plasma was ignited at 1 Pa in our helicon-type reactor and is characterized using optical emission measurements (optical actinometry) and electrical measurements, namely Langmuir and catalytic probe. By comparing catalytic probe data obtained at the center of the chamber with optical actinometry results, an approximate calibration of the actinometry method as a semi-quantititative measure of H density was achieved. Coefficients for conversion of actinometric ratios to H densities were tabulated and provided in the table below. Best agreement with catalytic probe results was obtained for (Hβ, Ar750) and (Hβ, Ar811) actinometric line pairs. Additionally, concentrations of electrons and ions as well as plasma potential, electron temperature and ion fluxes were measured in the chamber center at different plasma powers using a Langmuir probe. Moreover,

a global model of inductively-coupled plasma was formulated using a compiled reaction set for H_2/Ar gas mixture. The model results compared reasonably well with the results on H atom and charge particle densities and a sensitivity analysis of important input parameters was conducted. After characterization of the reactor, Si wafers with PMMA and carbon layers were processed in low-pressure H2 plasma. Measurements showed that etching rates of PMMA film were much higher than amorphous carbon layers. This work was partially supported from the SPAM (Surface Cleaning for Advanced Manufacturing) Marie Curie project, and by a post-doctoral Fellowship program of the Serbian government supporting Nevena Puac.

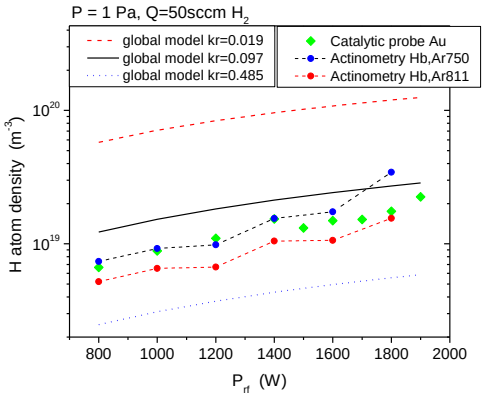

Fig.4. *Comparison of H density obtained from the global model for three different values of surface recombination coefficient and the catalytic probe and actinometry data.*

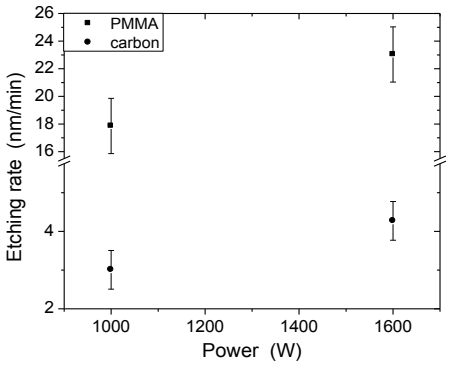

Fig.5. *PMMA (squares) and carbon (circles) layer etching rates dependence on power in H2 plasmas. Different samples used and processed for 5 min.*

Table III. Coefficients used for conversion of actinometric ratios to H densities.

Actinometry ratio used	λ-involved (nm)	Detector response ratio in our system	Ratio of A coefficients	γ	Actinometric conversion coefficient γ * k_{Ar}^{dir}/k_H^{dir} to convert intensity to concentration ratio of N_H/N_{Ar}.					
					2eV	2.5	3eV	3.5	4eV	4.5
Hα/Ar750	656/750	0.7	2.2	1.4	0.25	0.31	0.36	0.41	0.44	0.48
Hα/Ar811	656/811	0.4	2.3	0.8	0.19	0.20	0.22	0.22	0.23	0.23
Hβ/Ar750	486/750	1.7	3.6	3.9	3.55	4.16	4.70	5.19	5.60	5.99
Hβ/Ar811	486/811	1.1	3.6	2.2	2.62	2.71	2.78	2.83	2.85	2.87

A.4 Nanoscale silicon etching: High aspect ratio silicon nanowire fabrication using colloidal self-assembly as a masking layer

A. Smyrnakis, A. Zeniou, E. Gogolides, A. Tserepi

High aspect ratio perpendicular to the substrate silicon nanowires (SiNWs) as well as micro- or nanopillars with controlled sizes and period are of extreme interest due to their structural, electrical and optical properties and their possible application in photovoltaics, sensors and energy harvesting devices. For the fabrication of such features, we developed a cryogenic silicon etching process that uses a SF_6/O_2 gas mixture at cryogenic temperature (T<−100 °C) and a time multiplexed deep reactive ion enhanced (DRIE) etching process at room temperature using one cycle of SF_6 followed by a C_4F_8 cycle. For the patterning, we use either the cost effective process of colloidal particle self-assembly (polystyrene micro particles serving as etch mask), optical lithography or e-beam lithography. We further optimize and improve our silicon etching process to reach as high aspect ratio as possible. Fabrication process offers full versatility in wire/pillar pitch, diameter and height, showing high anisotropy and etch rate, clean, smooth and controllable sidewall profile. Sub-200 nm diameter SiNWs with high aspect ratio up to 100:1 are demonstrated.

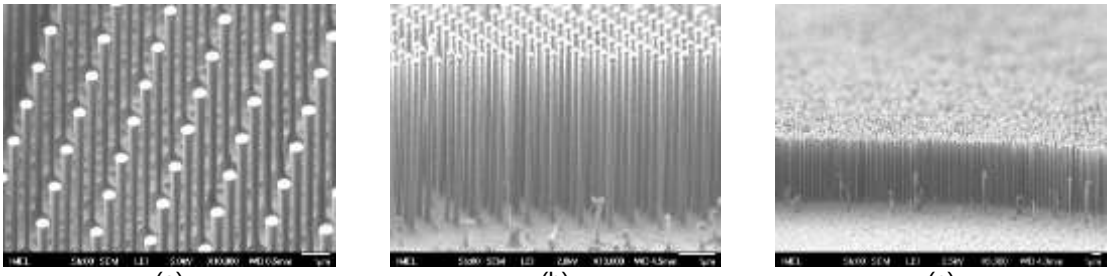

(a) (b) (c)

Fig.6. *(a) SEM image of ordered SiNWs fabricated by optical lithography followed by cryogenic plasma etching process. The diameter of the wires is ~450 nm with an aspect ratio of 17:1. (b)-(c) SEM image of SiNWs fabricated by colloidal lithography followed by cryogenic plasma etching process. The diameter of the wires is ~200 nm with an aspect ratio of 26:1 and 37:1 respectively.*

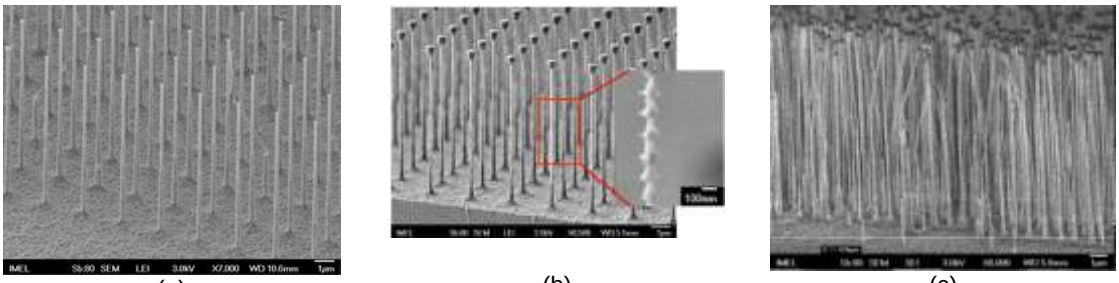

(a) (b) (c)

Fig.7. *(a) SEM image of ordered SiNWs fabricated by e-beam lithography followed by time multiplexed DRIE plasma etching process. The diameter of the wires is ~200 nm with an aspect ratio of 40:1. (b)SEM image of SiNWs fabricated by optical lithography followed by time multiplexed DRIE plasma etching process. The diameter of the wires is ~100 nm with an aspect ratio of 46:1. (c)SEM image of SiNWs fabricated by colloidal lithography followed by time multiplexed DRIE plasma etching process. The diameter of the wires is ~100 nm with an aspect ratio >100:1.*

Reduction of optical reflection is important for many technologies including solar energy, photodetectors, and high-contrast, antiglare and stealth surfaces. In order to examine the optical properties of our silicon nanowires and evaluate their possible use in photovoltaic devices, we performed reflectance and FTIR measurements. Using a reflection probe we measure the Specular Reflectance as a percentage (%R) relative to the reflection from a standard reference substance. Fig.6 presents, the specular reflectance of silicon surface with high aspect ratio perpendicular SiNWs of different diameter (d), height (h), period (a), where low reflectance is identified. The characteristics of the SiNWs are mentioned in the text box embedded. We note that those samples were fabricated by the colloidal lithography that gives hexagonally packed wire arrays, and the cryogenic process was used for the silicon etching. Fig.7 shows the transmittance in the near/mid infrared regime of Si pillars of the same diameter and height but of different period (2 um and 3 um) of a square lattice. The pillars show characteristics minima in NIR Transmittance showing interest in the NIR regime for applications such as sensors.

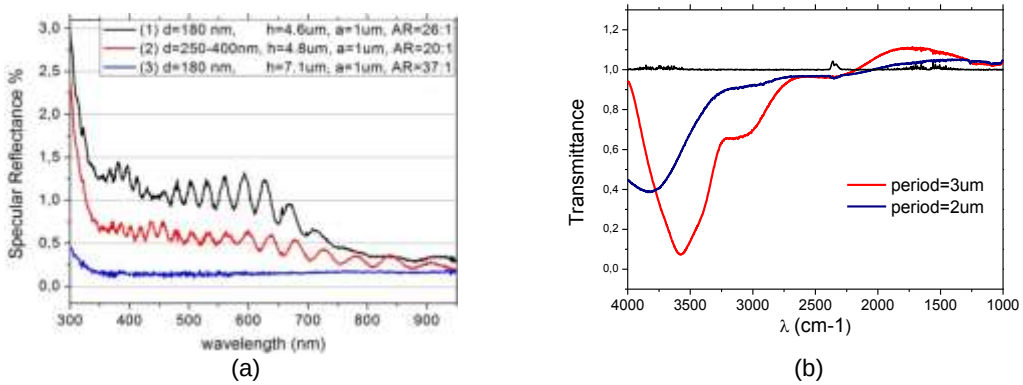

(a) (b)

Fig.8. *(a) Specular reflectance of silicon surface with perpendicular silicon nanowires (SiNWs) of different diameter, d, height, h, period, a. (b) Transmittance in the near/mid infrared regime of Si pillars.*

B. Nano Metrology – Characterization

B.1 Measurement of thickness of very thin films on plasma patterned spots by means of Atomic Force Microscopy

V. Constantoudis, A. Malainou, A. Tserepi and external collaborators

In many applications, plasma etching is used for the fabrication of closely packed spots with various geometries on a substrate and the selective chemical modification of their top surfaces. The measurement of the height of these spots may be critical since it may reveal the selective deposition of some material on these (for example proteins as is the case of the work reported in D.2.5 “Nanoscale protein patterning on Si substrates using colloidal lithography and plasma processing). A method which has been proposed for this measurement is to obtain the Atomic Force Microscopy topography of the pattern and the histograms of its heights. Ideally, the histogram would have two peaks, difference of which would give the average spot height. However, when the spots are densely patterned the AFM tip cannot follow the topography elevations and give reliable measurements of the substrate height (“flying tip effect”). To remedy this shortcoming, we proposed a method to control the flying tip effects by changing the relative orientation of tip scanning direction and spot arrangement. We have observed that when the scanning direction coincides with the post orientation then the flying tip effect is enhanced and the substrate peak in the histogram is broken down to the artifact peak and the real one (see Fig.9b). We have applied this technique with success in the measurement of the thickness of a protein monolayer (~2nm) deposited selectively on the top surfaces of SiO_2 spots developed on a Si substrate (see D.2.5 “Nanoscale protein patterning on Si substrates using colloidal lithography and plasma processing).

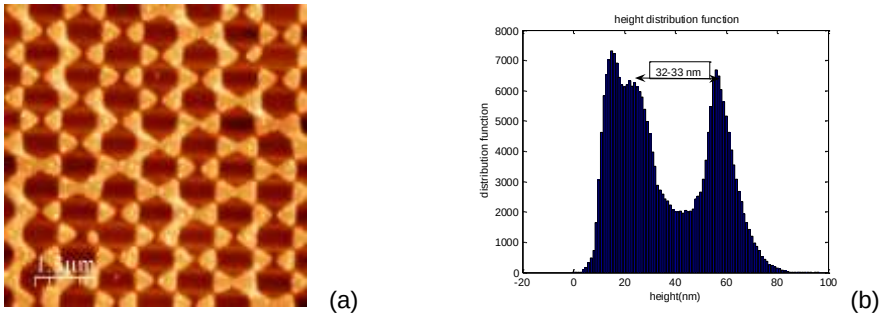

(a) (b)

Fig.9. *AFM image (a) and height histogram (b) of SiO_2 spots on Si substrate. Notice that due to the coincidence of the scanning direction with the post orientation the first peak of the histogram which corresponds to the Si surface is composed of two sub-peaks (Fig.9b). The first sub-peak is an artefact due to the “flying tip effect”, whereas the second peak corresponds to the actual Si background. Therefore, the height of the SiO_2nanoislands is measured approximately 32-33 nm in agreement with SEM measurement of the SiO_2nanoisland height.*

B.2 Evaluation of methods for noise-free measurement of edge roughness of lithographic line/space patterns using synthesized CD-SEM images

V. Constantoudis and external collaborators

The dimensions and edge morphology of the nanoscale patterns are usually measured from top-down Scanning Electron Images. This technique is widely applied in the measurement of the critical dimension and edge roughness of lithographic linear and circular features (Line Edge Roughness (LER) AND Contact Edge Roughness (CER)). The accuracy of the measurements is degraded due to the noise of the SEM measurement process. Since the measured quantities are at nanoscale regime, the evaluation of the noise effect is of paramount importance in nanometrology. The aim of the work reported here is to contribute to the understanding of the effects of noise on LER parameters when they are measured through the analysis of top-down CD-SEM images. To this end, first we have developed a methodology for the generation of synthesized CD-SEM images including resist lines with predetermined CD/pitch and LER parameters in which the noise level can be tuned at will (see Fig.10). The sources of noise can be the shot noise of SEM electron beam (Poisson-type) and the microscope electronics (Gaussian-type). Then we have used the generated CD-SEM images to evaluate three methods devised and proposed for the reduction of noise effects and the

extraction of noise-free LER/LWR parameters. The first method (called fractal method) is presented for first time, while the next two (model filtering and Power Spectral Density) have been already proposed and applied in literature. We found that the all methods are able to reproduce the true RMS value except for the cases with high signal to noise ratio and small input RMS (0.5nm) or correlation length (10nm). The reduction of the noise effects on ξ, α and the prediction of their true values seems to be more difficult, although at low noise levels successful predictions are achieved by both methods (fractal and PSD) especially for the correlation length ξ.

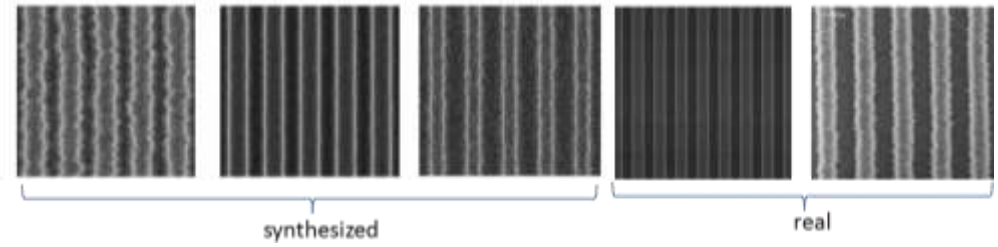

Fig.10. *Three examples of synthesized images generated by the algorithm described in the text for different choices of input parameters. Notice their apparent similarity with real top-down SEM images of line/space patterns (typical examples are also shown in the Figure)*

B.3 Alternative methods for the characterization of the morphology of nanostructures: Rough surfaces as complex networks

N. Karasmani, V. Constantoudis

The measurement and characterization of the degree of periodicity and order in a surface is critical especially in self-assembled nanostructures. Conventional tools for periodicity detection and evaluation suffer from their own limitations. For example, Fourier transform due to the kernel of harmonic waves it implies is not only sensitive to the degree of periodicity but also to the shape of the repeated structure. The above limitations motivate us to seek alternative methods for the characterization of surface roughness. To this end, we employed the recent advances in complex network theory and critically examined the benefits of their application in roughness characterization. The key idea here is to transform a surface to a network by considering the measured grid points of the surface as the nodes of the network and the link between two nodes inversely proportional to the difference of their heights (Height-Similarity Method, see Fig.11a). After the application of this method to totally random and self-affine surfaces, we proceeded this year to examine its sensitivity to the detection of the different kinds of deviations from periodicity. We considered surfaces consisting of identical Gaussian bumps in full periodic arrangements. The deviations from periodicity can be modeled either by changing randomly the position of the bumps (position-based deviation) or the bump shape (shape-based deviation). Fig.11b and Fig.11c shows the node-degree distribution of the networks generated by surfaces with position and shape-based deviation from full periodicity respectively. The graphs demonstrate the sensitivity of the degree distribution to the kind of the deviation from periodicity and motivate us for further investigation of the prospects of the network approach to morphology characterization.

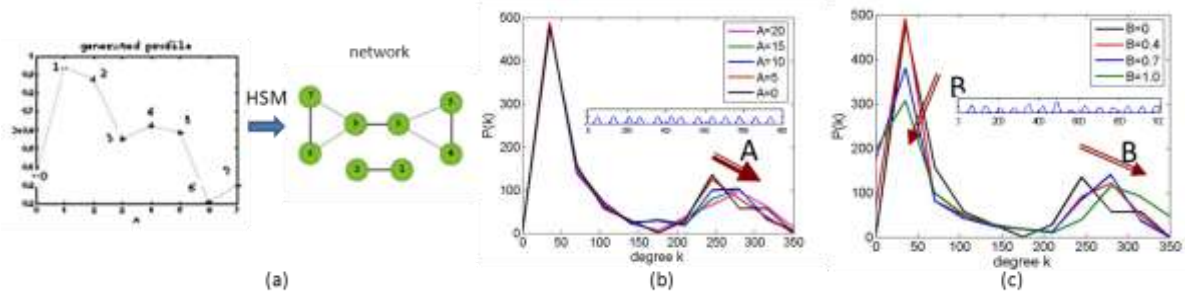

Fig.11. *(a) Schematic of the Height Similarity method for the generation of a network from a rough profile, (b) and (c) the degree distribution of the network nodes for surfaces with increased position and height-based deviation from periodicity respectively.*

C. Modeling – Simulation

C.1 Modeling of Line Edge Roughness transfer during plasma etching: Comparison with experiments and rules of thumb

V. Constantoudis, G. Kokkoris, E. Gogolides

The main application of plasma technology in microelectronics is the transfer of the resist patterns formed with some kind of lithography (optical, electron, nanoimprint, colloidal, etc.) to the substrate(s). When the dimensions of the transferred pattern are in the nanoscale regime then any kind of deviation from the ideal shape in the final pattern (Line Edge Roughness, sidewall slope and shape) becomes critical and should be under control. The contributions to these deviations mainly come from the resist sidewall roughness and profile shape and the plasma etching transfer process. In order to evaluate these contributions and help their control, our group has proposed some years ago a geometrical model of pattern transfer process which takes into account a detailed representation of resist sidewall roughness and profile shape while considers a simple anisotropic ion-driven etching process for pattern transfer. The first results and predictions of this model and its 3D extension have been presented in the reports of the previous years.
During this year, we have proceeded to a systematic comparison of model predictions with the available in literature experimental results. The comparison was mainly focused on the LER rms value (3σ) and power spectrum. As we can see in Fig.12 for rms, modeling results reproduce the experimental trends and behavior with high fidelity. Similar agreement has been observed in the transfer of the power spectra of sidewall roughness.

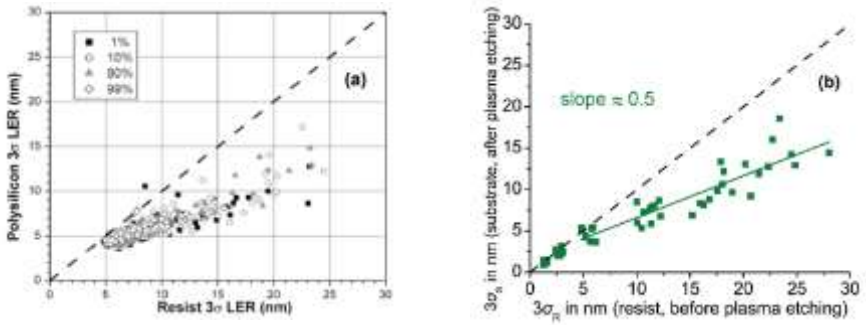

Fig.12. *Experimental (a) and modeling (b) results for the substrate LER after pattern transfer (3σS) versus the resist LER before pattern transfer (3σR). The modeling results are taken for resist thickness 150nm, correlation length 30nm, roughness exponent 0.6, etching depth150nm and resist profile slope 86.2o. Notice the almost quantitative agreement of the model predictions and experimental measurements.*

Furthermore, inspired by the model we have devised some rules of thumb governing the pattern transfer etch process. The most important regards the necessary condition for getting LER reduction after pattern transfer. According to this the resist roughness and shape parameters σ_R *(rms value),* ξ_R (correlation length) and $\tan\theta_R$ (sidewall slope) should obey the condition: $(\sigma_R/\xi_R)\tan\theta_R > 1/c$ where c=2.5-3.

C.2 Global modeling of plasma reactors: Application in Hydrogen cleaning plasmas

N. Skoro, S. Mouchtouris, G. Kokkoris, E. Gogolides

A global (0d) model for H_2/Ar plasma was formulated including both gas phase and surface reactions (c.f. Table IV). The model results were compared (cf. section A.3) with measurements for H density coming from catalytic probe and actinometry and for electron density and temperature coming from Langmuir probe. Good agreement between experimental and modeling results was found. The important model parameters were extracted and a sensitivity analysis was performed. Using realistically calculated surface recombination coefficient, the model results were compared well with the measured H density. The sensitivity analysis showed that H density strongly depended on the surface recombination coefficient. Additionally, there was an agreement of model results with the measured electron temperature. The potential sources of the difference between the model results with the measured electron density were investigated by the sensitivity analysis: electron density was found to be sensitive to the rate coefficients of electronic excitation leading to H_2 dissociation and ionization of H_2. In

addition to the latter coefficients, the surface recombination coefficient of H, and the cross section for ion – neutral collisions in the plasma, which is important for the losses of ions at the wall surfaces, were found to be the most important model parameters.

Table IV. Gas phase (G) and surface (S) reactions for the global model of H_2/Ar plasma.

G1	$H_2(X^1\Sigma_g^+) + e \rightarrow H_2(b^3\Sigma_u^+) + e \rightarrow 2H + e$	G12	$H_2^+ + e \rightarrow H^+ + H + e$	G23	$ArH^+ + e \rightarrow Ar + H$
G2	$H_2 + e \rightarrow H_2(B^1\Sigma_u^+) + e$	G13	$H_2^+ + e \rightarrow 2H^+ + 2e$	G24	$H_2^+ + H_2 \rightarrow H_3^+ + H$
G3	$H_2 + e \rightarrow H_2(C^1\Pi_u) + e$	G14	$H_2^+ + e \rightarrow 2H$	G25	$Ar(met) + H_2 \rightarrow Ar + 2H$
G4	$H_2 + e \rightarrow H_2(c^3\Pi_u) + e \rightarrow 2H + e$	G15	$H_3^+ + e \rightarrow H^+ + 2H + e$	G26	$Ar(met) + Ar \rightarrow 2Ar$
G5	$H_2(X^1\Sigma_g^+, v=0) + e \rightarrow H_2(X^1\Sigma_g^+, v=1) + e$	G16	$H_3^+ + e \rightarrow H_2 + H$	G27	$Ar^+ + H_2 \rightarrow Ar + H_2^+$
G6	$H_2 + e \rightarrow H_2(v=2) + e$	G17	$H + e \rightarrow H^+ + 2e$	G28	$Ar^+ + H_2 \rightarrow ArH^+ + H$
G7	$H_2 + e \rightarrow H_2(v=3) + e$	G18	$Ar + e \rightarrow Ar + e$	G29	$ArH^+ + H_2 \rightarrow H_3^+ + Ar$
G8	$H_2 + e \rightarrow H(n=3) + H + e$	G19	$Ar + e \rightarrow Ar(met) + e$	G30	$H_3^+ + H_2 \rightarrow H_3^+ + H_2$
G9	$H_2 + e \rightarrow H_2^+ + 2e$	G20	$Ar + e \rightarrow Ar^+ + 2e$	S1	$H \rightarrow \frac{1}{2} H_2$
G10	$H_2 + e \rightarrow H + H^+ + 2e$	G21	$Ar + e \rightarrow Ar + e$		
G11	$H_2 + e \rightarrow H_2 + e$	G22	$Ar(met) + e \rightarrow Ar + e$		

C.3 Modeling of the stochastic and topology effects on Contact Edge Roughness dependencies

V. M. Kuppuswamy, V. Constantoudis, E. Gogolides

In nanofabrication, stochastic effects coming from the discrete nature of materials (molecular structure) and of the fabrication means (photons, electrons, ions) induce roughness on the sidewalls of patterned features and variability of their sizes. At the same time, nanofeatures are usually closely packed and proximity inter-feature effects on their morphology should be taken into account (proximity effect). To evaluate the combination of these effects on the sidewall nanoroughness, we developed a modeling framework taking into account both stochastic and proximity effects. The motivation for this model was experimental results described in the Report of 2011 for the dependence of the sidewall roughness of contacts (Contact Edge Roughness) opened by Extreme Ultraviolet Lithography on the exposure dose. Analysis of these results revealed an increase of RMS with exposure dose and contact diameter (CD) (see Fig.13a) contrary to the expectations according to which the RMS value of the sidewall roughness of resist features should go down with the square root of the exposure dose i.e. the number of incident photons (shot-noise effect). The modeling showed that the proximity effects play a significant role in CER dependence on dose due to the specific 2D topology of contacts; for dense contacts (small pitch) the growth of contact diameter with dose bring these closer especially along the lattice directions. This selective proximity increases the low frequency contact fluctuations and explains the CER increase with dose (see Fig.13b).

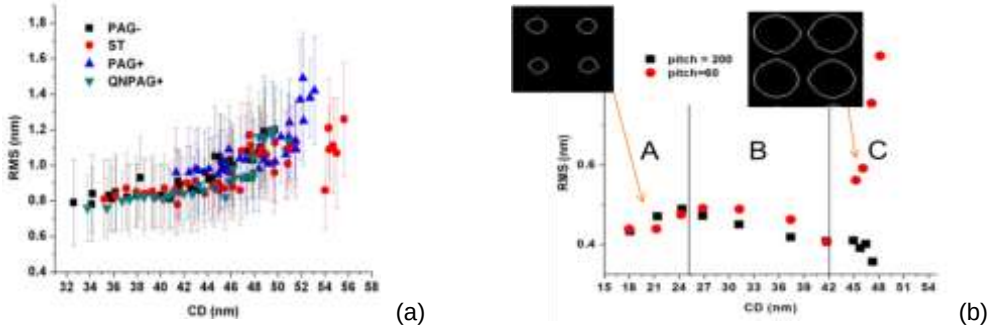

(a) (b)

Fig.13. *Experimental (a) and modelling results for the dependence of the RMS value of CER on the contact diameter (CD). The modelling results are for sparse (pitch=200nm) and dense (pitch=60nm) contact patterns. Notice that the experimental increase at high CD is reproduced only for the dense contacts revealing the critical role of the proximity effects between nearby contacts.*

C.4 Multiscale Computational Analysis of the Interaction between the Wafer Micro-Topography and the Film Growth Regimes in Chemical Vapor Deposition Processes

G. Kokkoris and external collaborators

The limiting step during the chemical vapor deposition (CVD) process of a film can be identified by the Arrhenius plot, which shows the effect of the wafer temperature on the deposition rate. The deposition limiting step, and as a consequence the Arrhenius plot, are affected by the operating conditions of the CVD reactor. By using a multiscale computational framework, it is shown that they are also affected by the existence of a micro-topography (e.g. micro-trenches) on the wafer. The origin of this effect is the loading phenomenon and the multiscale computations are used to quantify it: The deposition rate decreases in the diffusion limited regime; the latter and the transition regime are shifted at lower temperatures compared to the flat wafer case. The evolution of the deposited film profile in the micro-trenches is calculated at all deposition regimes. The film conformality starts to decrease when the wafer temperature exceeds the maximum temperature of the reaction limited regime. Finally, it is shown that the effect of the micro-topography on the species concentrations in the reactor bulk is important only in the transition regime (c.f. Fig.14). The case studies are CVD of a) tungsten from tungsten hexafluoride and b) silicon from silane.

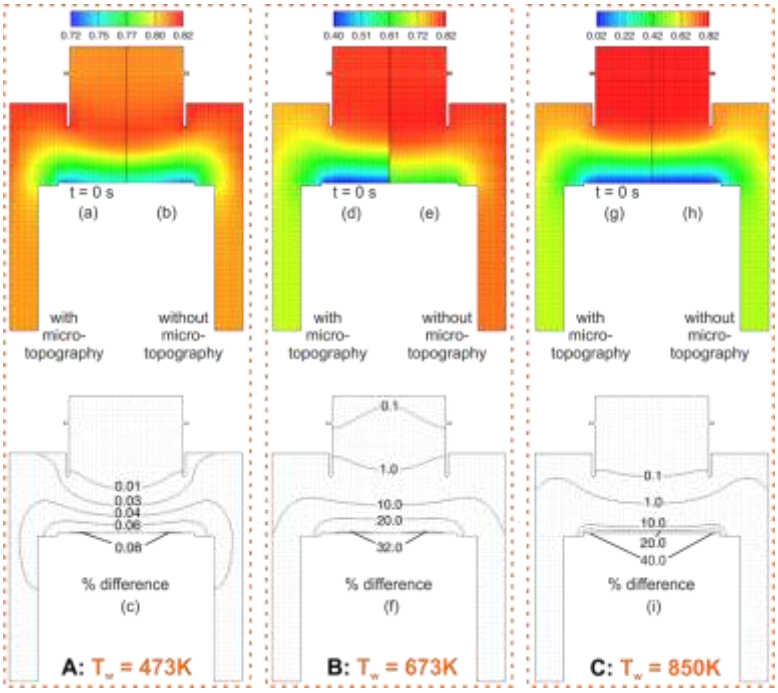

Fig.14. *CVD of W - mass fraction (of WF_6, which is the precursor) and % difference of the mass fraction inside the reactor. Column A (Tw = 473 K) corresponds to reaction limited regime, B (Tw = 673 K) to transition regime, and C (Tw = 850 K) to diffusion limited regime. (a), (d), and (g) show mass fraction with micro-topography at t=0 s. (b), (e), and (h) show the mass fraction without micro-topography. (c), (f), and (i) show the % difference between the cases with and without micro-topography.*

C.5 Ballistic and molecular dynamics simulations of aluminum deposition in micro-trenches

G. Kokkoris and external collaborators

Two different feature scale modeling frameworks are utilized for the study of aluminum (Al) deposition profiles inside micro-trenches. The first framework, which is applied in metal-organic chemical vapor deposition (MOCVD) of Al, couples a ballistic model for the local flux calculation, a surface chemistry model, and a profile evolution algorithm. The calculated conformity of the deposited film is compared with experimental results corresponding to Al MOCVD from dimethylethylaminealane (DMEAA). The outcome of the comparison is that the effective sticking coefficient of DMEAA is in the range of 0.1 – 1. There is also a strong indication that surface reaction kinetics follows Langmuir – Hinshelwood or Eley – Rideal mechanism. The second framework, which is applied in physical vapor deposition of Al, implements 2D molecular dynamics (MD) simulations. The simulations are performed in a “miniaturized” domain of some hundreds of Angstroms and are used to explore micro-trench filling during magnetron sputtering (MS) deposition of Al on a rotated substrate. Most of the experimental results are qualitatively reproduced by the MD simulations; the rotation, aspect ratio, and kinetic energy effects are correctly described despite the completely different length scales of simulation and experiment. The sticking probability of Al is calculated 0.6 for the conditions of the experiments.

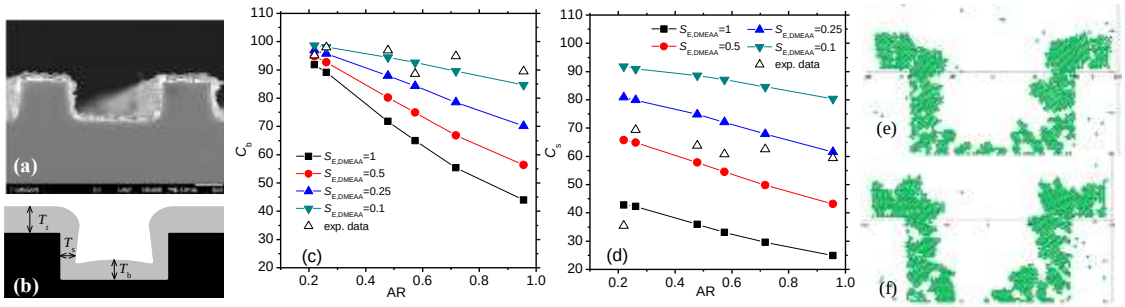

Fig.15. *(a) SEM image from a film profile in a trench with width equal to 3 μm. (b) Parameters used for the calculation of bottom (C_b) and sidewall (C_s) conformity: $C_x = T_x/T_t$ 100% (x=b, s). (c) C_b and (d) $C_s$vs trench AR. 2D MD simulations of Al MS deposition on Si trenches with AR=0.5. 3200 atoms are launched: (e) Ts= 300 K (surface temperature) and Ek = 0.026 eV (energy of depositing atoms) and (f) Ts= 300 K and Ek = 1 eV.*

C.6 Numerical calculation of the energy barrier for the transition from the Cassie-Baxter to Wenzel state on hydro(oleo)phobic surfaces

G. Kokkoris and external collaborators

The aim is to find the surface morphology (geometric pattern) which favors heterogeneous wetting (Cassie-Baxter, CB) state and exhibits increased resistance to fully wetting (Wenzel, W) state under the effect of disturbances induced by pressure, temperature, or electrical field. The resistance of a surface morphology to fully wetting state comes from the energy barrier that we have to overcome to get from the CB to the W state. In this work, a methodology for the calculation of the energy barrier for a simple system consisting of one droplet lying on one pillar is described. The effect of the shape of the pillar on the energy barrier is sought. The core of the methodology is the numerical solution (by the Galerkin/finite element method) of the Young Laplace equation which gives us the shape of the droplet on the pillar. The first step of the methodology is the continuation of the solution branch (Fig.16a) which shows that multiple equilibrium states exist for the same contact angle (θ_Y). The energy barrier comes from the energy difference between the unstable equilibrium state (U) and the CB state. For droplets with small volume (<10μl), the energy barrier is $\gamma_{LV}(A_{LV,U} - A_{LV,CB}) - \gamma_{LV}(A_{SL,U} - A_{SL,CB})\cos\theta_Y$ (γ is the interfacial tension and A is the interfacial area, L,V,S stand for liquid, vapor, solid). Thus, if we know the shape of the droplet at the different equilibrium states for a specific contact angle, we can calculate the energy barrier for this contact angle. The calculations show that the energy barrier increases with the aspect ratio (AR) and the sidewall slope of the pillar (Fig.16b) and decreases with the droplet to pillar volume ratio (V_d/V_p). The energy barrier is greater for pillars with negative slope compared to pillars with positive slope (Fig.16c).

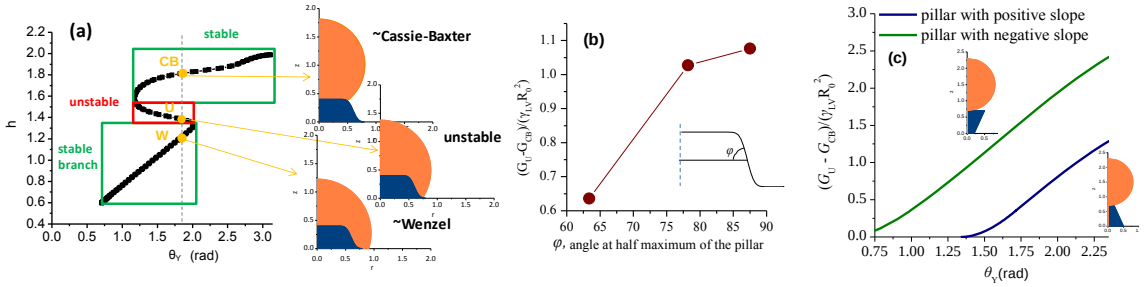

Fig.16. *(a) Continuation of the solution branch: The maximum height (z coordinate) of the droplet vs. the Young contact angle. 2 stable and 1 unstable braches of the solution are shown. (b) Energy barrier from CB to W state for a specific contact angle as a function of slope of a pillar with positive slope (V_d/V_p=5, AR=0.5). (c) The energy barrier for pillars with positive and negative slope vs. θ_Y (V_d/V_p=7, AR=1). G_U, G_{CB} are the energies of the unstable and CB states. R_0 is a length constant to make the energy barrier unitless.*

D. Applications

D1. "Smart" Nanostructured Surfaces

D1.1 Hydrophobic coatings and monolayers on flat plasma oxidized polymeric surfaces

K. Ellinas, G. Boulousis, E. Gogolides, A. Tserepi and external collaborators

Here, we compared different techniques for polymeric surface hydrophobization following a mild plasma oxidation. We established the use of fluorinated SAMs (PFOTS-perfluorinated octyl trichloro silane self assembled monolayers) by two different coating processes (wet & dry) and compared their wetting properties versus aplasma deposited fluorocarbon coating. In the following Table V, we present the static contact angle of different test liquids on three different coatings. As clearly see the PFOTS monlayers have improved performance compared to plasma deposited teflon-like fluorocarbon coatings, at least as far as contact angle increase is concerned.

Table V. Contact angles of PFOTS and plasma deposited fluorocarbon layers

Flat PMMA substrate		Wet deposited PFOTS	Dry deposited PFOTS	Plasma deposited C_4F_8
After grafting	Water	125 (15° hysteresis)	119	110
	Soya oil	90	88	62
	Hexadecane	75	72	41

D1.2 Hierarchical, oxygen plasma nanotextured, superoleophobic polymeric surfaces with random or ordered nanostructures

K. Ellinas, G. Boulousis, E. Gogolides, A. Tserepi and external collaborators

We fabricated two types of superoleophobic surfaces. Random, plasma nanotextured surfaces were simply etched in oxygen plasma. Ordered, plasma nanotextured surfaces were first coated with polysterene microspheres and then etched and nanotextured in an oxygen plasma (see Fig.17). Hydrophobization of both surfaces followed using the PFOTS wet deposited monolayers (see D1.1 above). Dynamic contact angle measurements on micro - nano textured PMMA and PEEK after 20 min O_2 plasma treatment and subsequent FDTS grafting are provided in Table VI. Superolephobicity is observed for all liquids tested, and a significant improvement compared to fluorocarbon plasma deposited coatings (using C_4F_8 plasma). These findings of the current study are consistent and slightly improved (PMMA 20min surface) from those superoleophobic surfaces reported in the literature for similar techniques.

Table VI. The static, advancing, receding contact angles and hysteresis are shown for water, soya oil and hexadecane on silane modified hierarchical randomly rough plasma nanotexturedsurfaces of PMMA.

Liquid	Contact angle	**PMMA 20 min O_2plasma**
Water	Static	167
	Adv/Rec(Hyster)	168/166 (2°)
SoyaOil	Static	157
	Adv/Rec(Hyster)	157/153 (4°)
Hexadecane	Static	142
	Adv/Rec(Hyster)	145/135 (10°)

* 5 μL liquid, error in Static ±2° advancing and receding ±5° (hysteresis is shown in parenthesis)

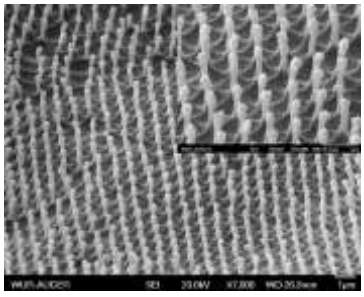

(a)

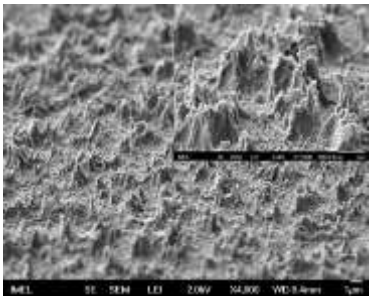

(b)

(c)

Fig.17. *(a) 60 degrees tilted SEM images of the hierarchical, ordered hexagonical packed pillar-like structured surfaces using 1 μm PS particles followed by plasma etching (b) 10 min plasma nanotextured PMMA surface after the silanization process (c) Various liquid drops (water, diiodomethane, soya oil) on superoleophobic PMMA surfaces*

D1.3 Hierarchical, SF_6 plasma nanotextured, superhydrophobic PDMS surfaces with random nanostructures: Effect of PDMS thickness

M.-E. Vlachopoulou, E. Gogolides, A. Tserepi

The effect of PDMS substrate thickness on the SF_6-plasma induced nanoroughness and consequently on superhydrophobicity was investigated. In Fig.18, the evolution with plasma etching time of PDMS nanoroughness height is presented for different PDMS film thicknesses, revealing the roughness decrease for increasing film thicknesses. Measurements of water contact angle on nanoroughened PDMS surfaces after the deposition of ~20nm fluorocarbon (FC) film reveals that superhydrophobic (SH) surfaces are obtained only in the case of very thin PDMS films, while thicker PDMS substrates present larger values of CA hysteresis (see Table VII). However, if the same surfaces are immersed in deionized water and dried, the CA hysteresis is drastically reduced, rendering all substrates superhydrophobic. This can be attributed to the induced modification of the surface topography as a result of wetting and drying and constitutes an interesting approach of making PDMS substrates superhydrophobic, independently from their thickness.

Table VII.

15 min SF_6	Without immersion			With immersion		
Thickness	Static (°)	Advancing (°)	Hysteresis (°)	Static (°)	Advancing (°)	Hysteresis (°)
20 μm	145	153	8	145	151	1
0.5 mm	145	146	11	147	154	4
2 mm	137	152	28	147	152	6

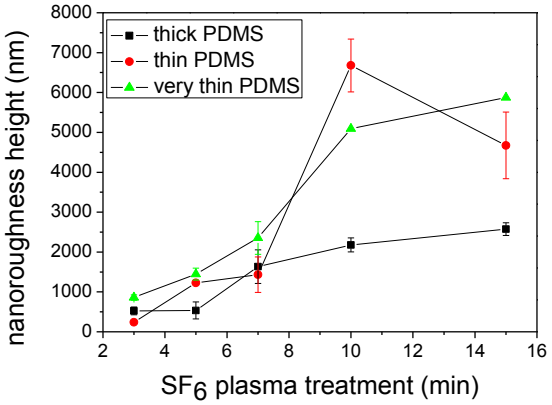

(a)

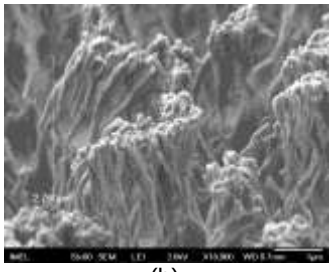

(b)

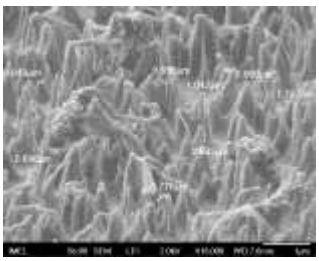

(c)

Fig.18. *(a) PDMS roughness height evolution with etching time for different PDMS film thicknesses: ~2 mm (thick PDMS), ~0.5 mm (thin PDMS) and ~ 20 μm (very thin PDMS) and SEM images of 15 min SF_6 treated thin PDMS before (b) and after (c) immersion in DI water*

D2. Microfluidics – Lab on Chip for Life Sciences (see also project III.2)

D2.1 Comparison of pressure drop in Superhydrophobic and superhydrophilic, hierarchical, plasma-nanotextured polymeric microchannels sustaining high-pressure flows

D. P. Papageorgiou, K. Tsougeni, A. Tserepi, E. Gogolides

We fabricated superhydrophilic and superhydrophobic polymeric microfluidic devices with controlled hierarchical, random roughness, using plasma processing. We implemented a dye staining technique to visually demonstrate the persistence of the superhydrophobic state under flow for pressures in excess of 2.5 bar inside the microchannel. We further confirmed the stability of superhydrophobicity by pressure drop measurements, friction factor and slip length calculations under laminar flow conditions. We also compared identical rough superhydrophilic and superhydrophobic microchannels showing reduced pressure drop in the latter by as much as 22 %. Plasma etching and simultaneous nanotexturing (followed by optional fluorocarbon plasma deposition) were thus shown as an easy-to-implement method for attaining robust Cassie-state against high-pressure microchannel flows.

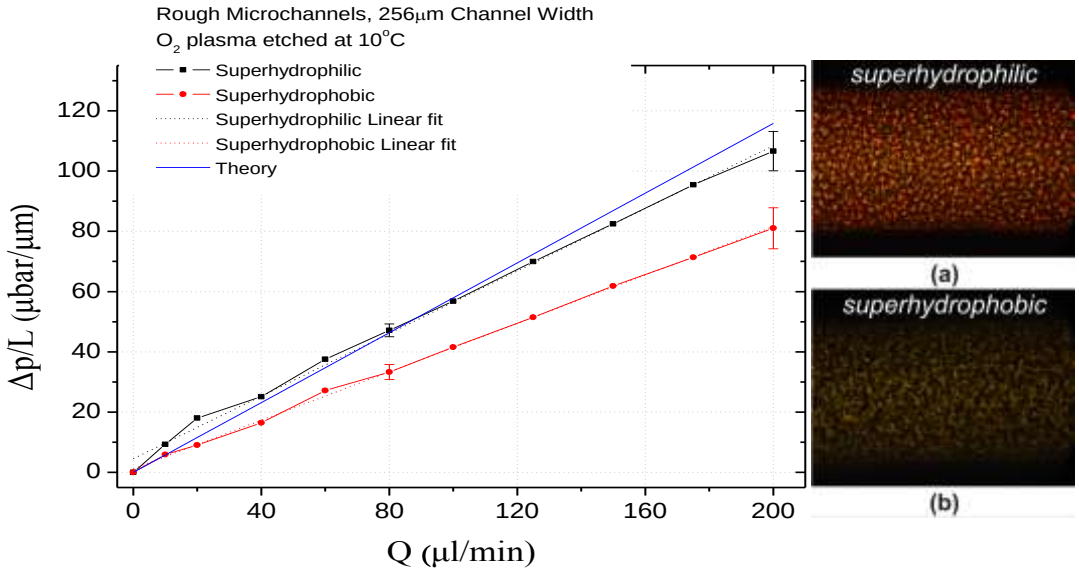

Fig.19. *Comparison of flow properties in rough superhydrophilic and superhydrophobicmicrochannels.(a) Pressure drop (μbar/μm) versus flow rate Q (μl/min). Mean values of three independent runs are shown for each curve. Diagrams correspond to 256μm wide, 25μm deep and 38.3mm long channels etched at 10 °C and stabilized with wetting. Data for other microchannels are shown in supporting information. Black lines correspond to superhydrophilic channels, and red lines to superhydrophobic ones. Dimensions of hierarchical micro-hills are: ~2-3 μm high, 1.5-4 μm wide, spaced 2-4 μm apart. Optical microscope dark-field images on stained superhydrophilic and syperhydrophobic microchannels. (a) Superhydrophilic microchannel is stained after red-dye flow. (b) Superhydrophobic microchannel is not stained after red-dye flow.*

D2.2 Comparison of flow field in superhydrophobic and superhydrophilic, hierarchical, plasma-nanotextured polymeric microchannels using micro PIV

K. Tsougeni, K. Ellinas, Th. Christoforidis, A. Tserepi, E. Gogolides and external collaborators

Plasma processing was used to roughen (texture) and control the wetting properties of polymeric Poly(methyl methacrylate) (PMMA) microchannels from superhydrophilic to superhydrophobic. A trapezoidal microchannel was used to provide three nanotextured walls (superhydrophilic or superhydrophobic). Particle Image Velocimetry (PIV) was then employed to monitor the velocity field, and observe the different flow behavior in the two wetting states during water flow. Using the ensemble PIV processing tool of the available software, several hundreds of images were analyzed in order to obtain the velocity field at various depths of each channel. Significant velocity was measured on the superhydrophobic walls.

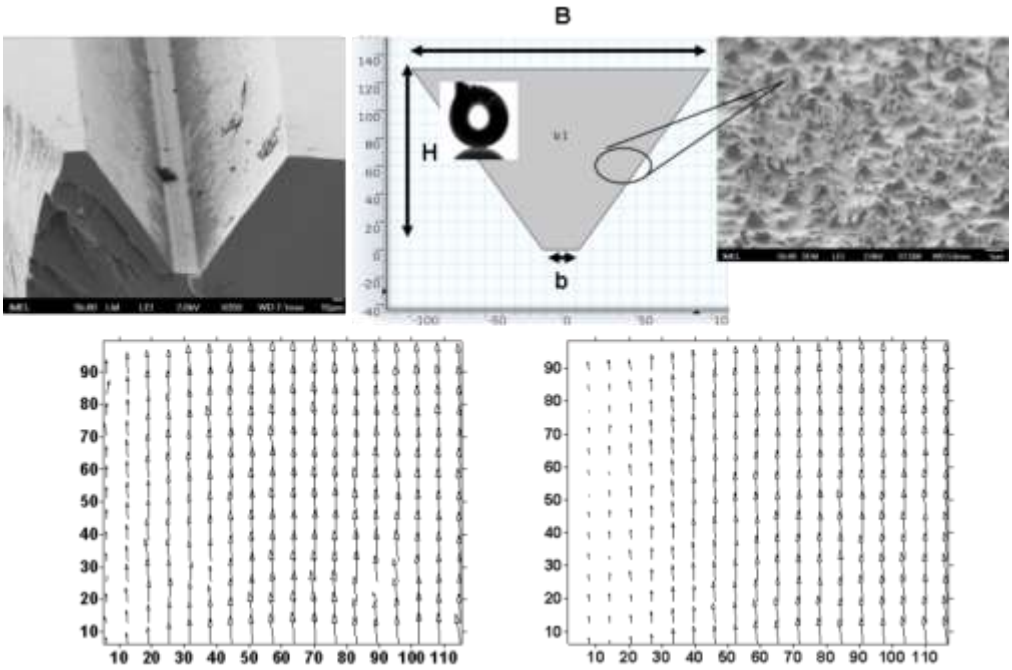

Fig.20. *Cross-section of an open microchannel with three superhydrophobic walls. Schematic of the cross-section and a zoom up of the rough walls. Velocity field comparison (dimensions in microns) of superhydrophobic (left) and superhydrophilic (right) microchannels showing higher liquid velocity on the superhydrophobic wall.*

D2.3 Phosphopeptide Enrichment and Separation in an Affinity Microcolumn on a Silicon Microchip: Comparison of Sputtered and Wet-Deposited TiO_2 Stationary-Phase

K. Ellinas, K. Tsougeni, G. Boulousis, A. Tserepi, E. Gogolides

We microfabricated a TiO_2 Affinity Chromatography microcolumn on silicon, comprising a deposited TiO_2 stationary phase, and demonstrated enrichment and separation of a standard mono-phosphopeptide with high capacity in this microcolumn. The TiO_2 stationary-phase is formed either with wet deposition or sputtering, and was found to be either amorphous (after sputtering), or crystalline (after sputtering and annealing or after wet deposition). All three methods of deposition (sputtering, sputtering and annealing, liquid deposition) provide enough capacity despite the non-porous nature of the deposited TiO_2. The chip design allows an expansion of its capacity (currently 1μg) by means of increasing the number of parallel microchannels at a constant sample volume. Our approach provides an alternative to off-line extraction tips (with typical capacities of 1 – 2 μg and sample volumes of 1 - 10 μL), and to on-chip efforts based on packed bed and frit formats using a standard material for MEMs and standard microfabrication techniques.

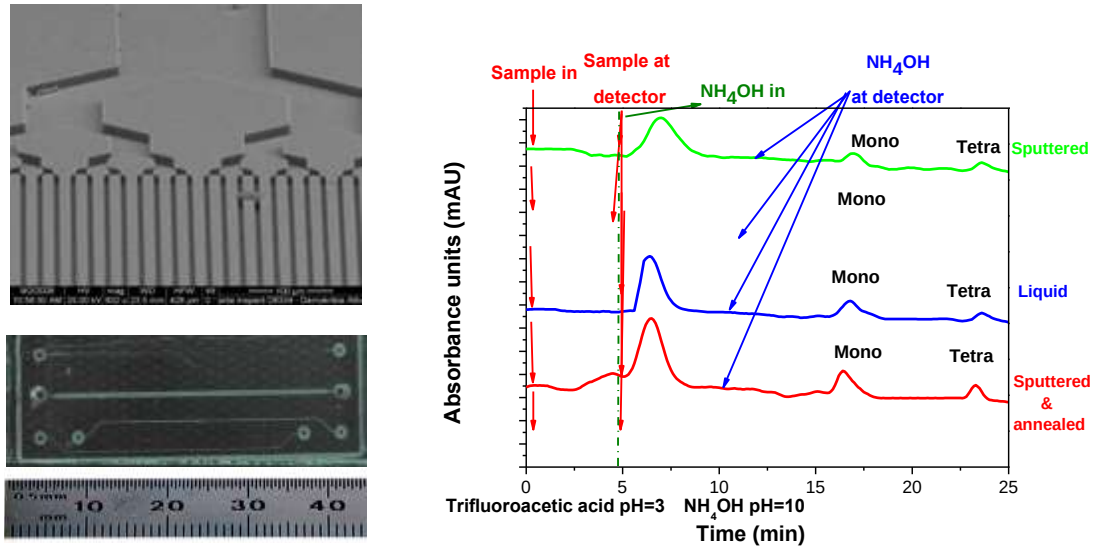

Fig.21. *(Left) Silicon microcolumn consisting of 32 parallel microchannels. (Right) Affinity chromatography on chip is shown, with retention, elution and separation of the peptide mixtures using the three different microcolumns. Some baseline shifts are due to shifting of the intensity of the Deuterium lamp. The sample quantity is 0.1nmol for each peptide (~0.2 μg for the mono-phosphopeptide, ~0.3 μg for the tetra-phosphopeptide and ~0.17 μg for the non-phosphorylated peptide).*

D2.4 Continuous-flow microfluidic device for DNA amplification (μPCR) on flexible polyimide substrate and integration in a Lab-On-Chip platform

D. Moschou, N. Vourdas, G. Kokkoris, G. Papadakis, S. Chatzandroulis, A. Tserepi

The development of a continuous flow μPCR device integrated with microresistors on a flexible polyimide (PI) substrate was continued this year further improving the device design and the fabrication process, while evaluating the robustness of the device and its performance for DNA amplification. A slightly modified device was proposed (microchannel of two different widths, depending on the desired sample residence time at each zone), and its behavior in respect to temperature uniformity was evaluated by means of numerical calculations. In addition, the fabrication process time and complexity were reduced, with the employment of photopatternable polyimide layers for the formation of microchannels by means of lithography. These improvements allowed us to evaluate the performance of our fabricated chips (Fig.22a) in respect to their DNA amplification efficiency (Fig.22b). Our devices achieved DNA amplification much faster (within a few minutes, depending on the sample flow rate) than conventional thermocyclers (a few hours). Building on the successful fabrication of microfluidics with photopatternable polyimide, we proceeded in developing a Lab-On-a-Chip platform on PCB substrates (Fig.23), integrating both a μPCR module and Si-based biosensors (placed in a cavity of the PCB, see image and inset), to allow DNA amplification and detection on the same chip.

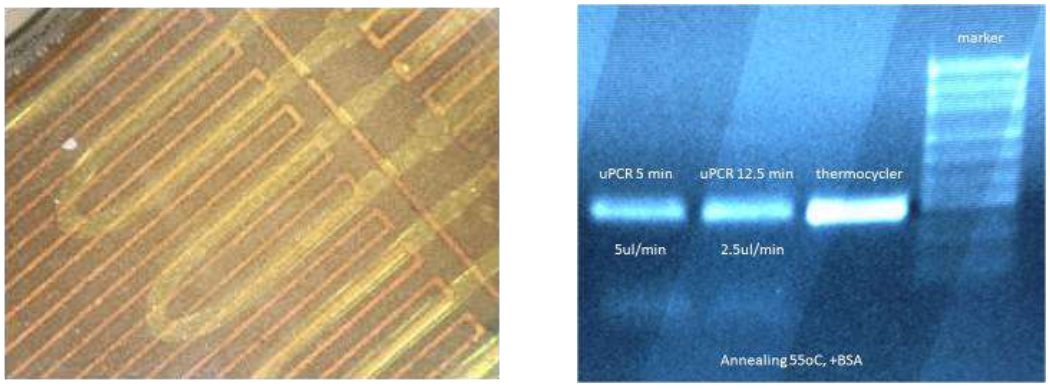

Fig.22. *(a) Fabricated μPCR chip with integrated microheaters (b) Demonstration of DNA amplification performed on our device and comparison with a commercial thermocycler (amplified DNA products on agarose gel).*

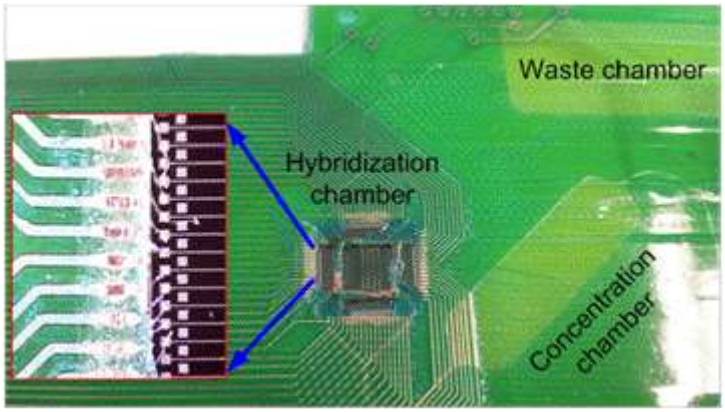

Fig.23. *Fabricated prototype of a Lab-On-a-Chip on PCB integrating a μPCR device and an array of Si-based biosensors*

D2.5 Nanoscale protein patterning on Si substrates using colloidal lithography and plasma processing

A. Malainou, K. Ellinas, V. Constantoudis, E. Gogolides, A. Tserepi and external collaborators

The potential of proteins to be integrated into micro or nanofabricated devices is steadily gaining importance for applications such as biosensors, bioMEMS, tissue engineering, and protein arrays. To create protein patterns, photolithography-based methods have been extensively used. However for features smaller than 1 μm, photolithography is reaching its limits, and becomes non cost-efficient. Moreover, dip-pen and e-beam lithography are serial processes and, as such, lack scalability. We propose a method for low-cost, large scale and high throughput, selective immobilization of proteins on nanopatterned Si, based on colloidal lithography and plasma processing in order to define the areas (< 300 nm) where proteins are *selectively* immobilized. A close-packed monolayer of PS microparticles is deposited on oxidized Si and, either after microparticle size reduction or alternatively after metal deposition through the PS close-packed monolayer, is used as etching mask to define SiO_2nanoislands (on Si, Fig.24). *Selective* protein immobilization on the SiO_2nanoislands occurs after plasma-induced chemical modification of the substrate. The thickness of the immobilized protein monolayer is estimated by means of detailed AFM image (Fig.25) statistical analysis. The method reported herein constitutes a cost-efficient route toward rapid, large surface, and high density patterning of biomolecules on solid supports that can be easily applied in BioMEMS or microanalytical systems.

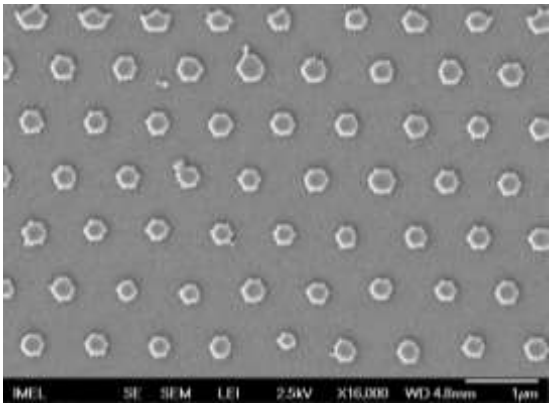

Fig.24. *SEM image of 300 nm SiO_2 nanoislands patterned on Si using colloidal lithography and plasma processing.*

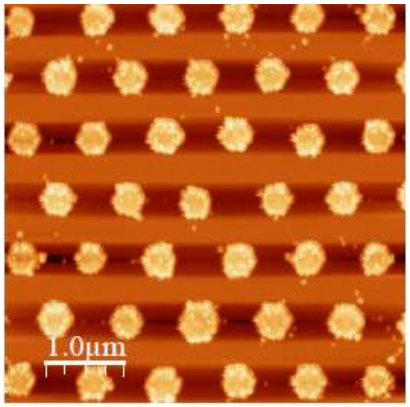

Fig.25. *Atomic Force Microscopy image of SiO_2 nanoislands on Si after selective immobilization of BSA on SiO_2 and not on Si surface.*

D3. Nano-Devices for Energy

D3.1 Devices for energy: Photovoltaic device based on Silicon Nanowires and Nanopillars

A. Smyrnakis, P. Dimitrakis, P. Normand, E. Gogolides

Recently, the potential application of high aspect ratio silicon nanowires (SiNWs) and nanopillars in solar cells was presented. The use of nanowires instead of bulk material or thin films provides opportunities to minimize losses of light absorption, in electron-hole generation and separation as well as in collection efficiency, and combine lower cost. We started our work on energy conversion devices by the fabrication of ordered silicon nanopillar arrays of different diameter and period with p-n junctions along the axial direction of each wire by colloidal lithography and plasma etching starting from a n-type Si wafer which was boron implanted to form a p-type surface layer. Electrical characterization of individual as well as bundle of nanopillars was performed in terms of I-V under light illumination, where promising first results were obtained in terms of short circuit current (I_{sc}) increase and filling factor (FF). The work will continue to the fabrication and characterization of the complete photovoltaic device and it will be extended to the fabrication of SiNWs solar cells with radial p-n junctions.

(a) 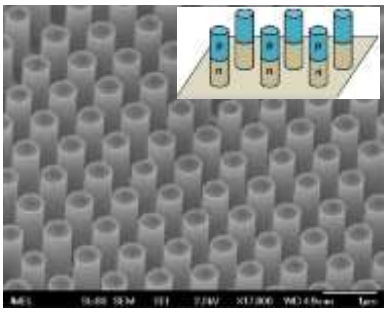 (b) 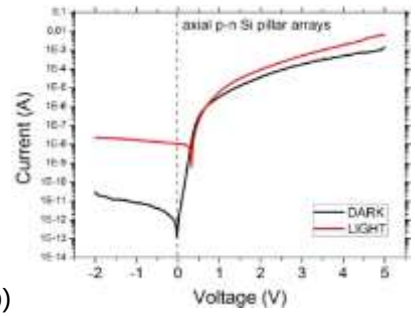

Fig.26. *SEM image of axially modulated p-n junction Si pillar arrays. Inset: The I-V response curve of the axial p-n Si pillar in dark and under illumination.*

PROJECT OUTPUT in 2012

Publications in International Refereed Journals

A. Plasma Nanofabrication

1. *Plasma directed organization of nanodots on polymers: Effects of polymer type and etching time on morphology and order,*
   Kontziampasis, D., Constantoudis, V., Gogolides, E.
   (2012) Plasma Processes and Polymers, 9 (9), pp. 866-872.

B. Nanometrology-Characterization

2. *Contact edge roughness metrology in nanostructures: Frequency analysis and variations,*
   Vijaya-Kumar, M.K., Constantoudis, V., Gogolides, E., Pret, A.V., Gronheid, R., (2012) Microelectronic Engineering, 90, pp. 126-130.
3. *Fractals and device performance variability: The key role of roughness in micro and nanofabrication,*
   Constantoudis, V., Patsis, G.P., Gogolides, E., (2012) Microelectronic Engineering, 90, pp. 121-125.

C. Modeling-Simulation

4. *The potential of ion-driven etching with simultaneous deposition of impurities for inducing periodic dots on surfaces,*
   Kokkoris, G., Gogolides, E.
   (2012) Journal of Physics D: Applied Physics, 45 (16), art.no. 165204
5. *Multiscale computational analysis of the interaction between the wafer micro-topography and the film growth regimes in chemical vapor deposition processes,*
   N. Cheimarios, G. Kokkoris and A. G. Boudouvis,
   (2012) ECS Journal of Solid State Science and Technology 1 P197-P203
6. *A consistent approach for the treatment of Fermi acceleration in time-dependent billiards,*
   Karlis, A.K., Diakonos, F.K., Constantoudis, V.,
   (2012) Chaos, 22 (2), art.no. 026120
7. *Quantum versus classical dynamics in a driven barrier: The role of kinematic effects,*
   Papachristou, P.K., Katifori, E., Diakonos, F.K., Constantoudis, V., Mavrommatis, E.,
   (2012) Physical Review E - Statistical, Nonlinear, and Soft Matter Physics, 86 (3), art. no. 036213
8. *Entropy analysis of word-length series of natural language texts: Effects of text language and genre,*
   Kalimeri, M., Constantoudis, V., Papadimitriou, C., Karamanos, K., Diakonos, F.K., Papageorgiou, H.
   (2012) International Journal of Bifurcation and Chaos, 22 (9), art. no. 1250223.

D1. "Smart" Nanostructured Surfaces

9. *Nanomechanical and nanotribological properties of plasma nanotexturedsuperhydrophilic and superhydrophobic polymeric surfaces,*
   Skarmoutsou, A., Charitidis, C.A., Gnanappa, A.K., Tserepi, A., Gogolides, E.
   (2012) Nanotechnology, 23 (50), art. no. 505711
10. *Hierarchical, plasma nanotextured, robust superamphiphobic polymeric surfaces structurally stabilized through a wetting-drying cycle,*
    Gnanappa, A.K., Papageorgiou, D.P., Gogolides, E., Tserepi, A., Papathanasiou, A.G., Boudouvis, A.G.
    (2012) Plasma Processes and Polymers, 9 (3), pp. 304-315
11. *Superior performance of multilayered fluoropolymer films in low voltage electrowetting,*
    Papageorgiou, D.P., Tserepi, A., Boudouvis, A.G., Papathanasiou, A.G.
    (2012) Journal of Colloid and Interface Science, 368 (1), pp. 592-598

D2. Microfluidics – Lab on Chip for Life Sciences

12. *Flame aerosol deposition of TiO2 nanoparticle films on polymers and polymeric microfluidic devices for on-chip phosphopeptide enrichment*,
    Rudin, T., Tsougeni, K., Gogolides, E., Pratsinis, S.E.
    (2012) Microelectronic Engineering, 97, pp. 341-344.
13. *High-capacity and high-intensity DNA microarray spots using oxygen-plasma nanotextured polystyrene slides*,
    Tsougeni, K., Koukouvinos, G., Petrou, P.S., Tserepi, A., Kakabakos, S.E., Gogolides, E., (2012) Analytical and Bioanalytical Chemistry, 403 (9), pp. 2757-2764.
14. *Creating highly dense and uniform protein and DNA microarrays through photolithography and plasma modification of glass substrates,*
    Malainou, A., Petrou, P.S., Kakabakos, S.E., Gogolides, E., Tserepi, A.
    (2012) Biosensors and Bioelectronics, 34 (1), pp. 273-281
15. *Controlled protein adsorption on microfluidic channels with engineered roughness and wettability*,
    Tsougeni, K., Petrou, P.S., Papageorgiou, D.P., Kakabakos, S.E., Tserepi, A., Gogolides, E.
    (2012) Sensors and Actuators, B: Chemical, 161 (1), pp. 216-222

Published Conference Proceedings

A. Plasma Nanofabrication

1. *Characterization of hydrogen based RF plasmas suitable for removal of carbon layers*,
   Škoro, N., Gogolides, E.
   (2012) Proceedings of 26th SPIG, August 27-31, 2012, Zrenjanin, Serbia, pp. 231

B. Nano Metrology – Characterization

2. *3d modeling of LER transfer from the resist to the underlying substrate: The effect of the resist roughness,*
   Kokkoris, G., Constantoudis, V., Gogolides, E.
   (2012) Proceedings of SPIE - The International Society for Optical Engineering, 8328, 83280V

C. Modeling – Simulation

3. *Contact edge roughness and CD uniformity in EUV: Effect of photo acid generator and sensitizer,*
   Kuppuswamy, V.-K.M., Constantoudis, V., Gogolides, E., VaglioPret, A., Gronhei, R.
   (2012) Proceedings of SPIE - The International Society for Optical Engineering, 8322, art. no. 832207
4. *Noise effects on contact edge roughness and CD uniformity measurement*,
   Constantoudis, V., MurugesanKuppuswamy, V.K., Gogolides, E.,
   (2012) Proceedings of SPIE - The International Society for Optical Engineering, 8324, art. no. 83240K.

D1."Smart" Nanostructured Surfaces

5. *Hierarchical, Plasma Nanotextured, Superamphiphobic Polymeric Surfaces*,
   K. Ellinas, K. Tsougeni, M. Vlachopoulou A. Tserepi, E. Gogolides
   (2012) Proceedings of 13th International Conference on Plasma Surface Engineering
6. *Development and characterisation of superhydrophobic α-alumina ceramic membranes with plasma surface nanotexturing*,
   Stathopoulos, V., Papandreou, A., Vourdas, N., Tserepi, A., Gogolides, E.
   Proceedings of Spring EMRS 2012 Meeting, May 14-18, 2012, Strasbourg, France

D2. Microfluidics – Lab on Chip for Life Sciences

7. *Fabrication of a label-free micromechanical capacitive biosensor and integration with μPCR towards a LoC for disease diagnosis,*
   D. Moschou, N. Vourdas, G. Kokkoris, G. Tsekenis, V. Tsouti, I. Zergioti, A. Tserepi, S. Chatzandroulis
   (2012) Proceedings of the 16th Int. Conference on Miniaturized Systems for Chemistry and Life Sciences (μTAS)
8. *Development of a continuous-flow μPCR device with microheatingelementsintegrated with biosensors towards a LoC system for disease diagnosis,*
   N. Vourdas, D. Moschou, G. Kokkoris, G. Papadakis, S. Chatzandroulis, A. Tserepi
   (2012) Proceedings of 3rd European Microfluidics Conference, paper no. 128
9. *Flow study in randomly-rough superhydrophilic and superhydrophobic plasma nanotexturedmicrochannels using micro-PIV*,
   K. Tsougeni, K. Ellinas, A. Glynou, T. Christoforidis, D.S. MathiouIakis, A. Tserepi, E. Gogolides
   (2012) Proceedings of 3rd European Microfluidics Conference, paper no. 132
10. *Control of flow and protein adsorption on plasma nanotextured microfluidics*,
    K. Ellinas, K. Tsougeni, P.S. Petrou, D.P. Papageorgiou, S.E. Kakabakos, A. Tserepi, E. Gogolides
    (2012) Proceedings of 3rd European Microfluidics Conference, paper no. 133

Conference Presentations

A. Plasma Nanofabrication

1. *High-aspect-ratio Si nanowire fabrication using Colloidal Self-assembly and fluorine-based plasma etching* (poster),
   A. Zeniou, A. Smyrnakis, E. Gogolides
   Plasma Etch and Strip in Microelectronics (PESM) March 15-16, 2012, Grenoble, France
2. *Characterization of Hydrogen-based Plasmas for Cleaning of Organic Contamination from EUV Optics* (poster),
   N. Škoro, E. Gogolides
   Plasma Etch and Strip in Microelectronics (PESM) March 15-16, 2012, Grenoble, France
3. *Plasma directed assembly: A new technology for polymer surface nanotexturing and applications* (oral),
   D. Kontziampasis, A. Bourkoula, A. Smyrnakis, P. S. Petrou, S. E. Kakabakos, E. Gogolides
   XI International Conference on Nanostructured Materials (NANO 2012) August 26-31, 2012, Rhodes, Greece

4. *Cleaning of Organic Contamination from EUV Optics Surfaces Using Hydrogen-based Plasmas* (poster),
   N. Skoro, E. Gogolides
   13th International Conference on Plasma Surface Engineering (PSE), September 10 - 14, 2012, Garmisch-Partenkirchen, Germany
5. *Plasma Directed Assembly: Process Issues, Materials and Applications* (poster),
   D. Kontziampasis, A. Smyrnakis, V. Constantoudis, E. Gogolides
   13th International Conference on Plasma Surface Engineering (PSE), September 10 - 14, 2012, Garmisch-Partenkirchen, Germany
6. *High aspect ratio, plasma etched silicon nanowires: Fabrication and optical property characterization* (oral),
   A. Smyrnakis, A. Zeniou, E. Almpanis, N. Papanikolaou, E. Gogolides
   38th International Micro & Nano Engineering Conference (MNE), September 16-20, 2012, Toulouse, France

B. Nano Metrology – Characterization

7. *Cyclo olefin polymer (COP) liquid chromatography microcolumns for reversed phase anf affinity separations* (poster),
   K. Tsougeni, A. Tserepi, E. Gogolides
   38th International Micro & Nano Engineering Conference (MNE), September 16-20, 2012, Toulouse, France

C. Modeling – Simulation

8. *Contact versus Line Edge Roughness in extreme ultra-violet lithography resists: Effects of exposure dose* (poster),
   V.K. Murugesan Kuppuswamy, V. Constantoudis, E. Gogolides
   38th International Micro & Nano Engineering Conference (MNE), September 16-20, 2012, Toulouse, France
9. *3D modeling of Line Edge Roughness transfer from the resist to the underlying substrate: The effect of resist roughness* (oral),
   G. Kokkoris, V. Constantoudis, E. Gogolides
   Plasma Etch and Strip in Microelectronics (PESM) March 15-16, 2012, Grenoble, France
10. *A crossbred multi-parallelmethod for accelerating multiscale computations in a chemical reactor analysis*,
    N. Cheimarios, I. Aviziotis, G. Kokkoris and A.G. Boudouvis
    6th European Congress on computational methods in applied science and engineering, ECCOMAS, Vienna, Austria, September 10-14, 2012
11. *Designing a non-uniform wafer micro-topography for uniform films in chemical vapor deposition processes,*
    N. Cheimarios, S. Garnelis, I. Aviziotis, G. Kokkoris and A. G. Boudouvis
    38th International Micro & Nano Engineering Conference (MNE 2012), Toulouse, France, September 16-20, 2012

D2. Microfluidics – Lab on Chip for Life Sciences

12. *Cell Attachment on Plasma Nanotextured PMMA Substrates* (poster),
    D. Kontziampasis, A. Bourkoula, P. Petrou, A. Tserepi, S. Kakabakos, E. Gogolides
    5th International Conference on Micro-Nanoelectronics, Nanotechnologies and MEMS, 7-10 October 2012, Kokkini Hani, Heraklion, Greece
13. *Integration of a label-free micromechanical capacitive biosensor in a LoC for disease diagnosis* (poster),
    D. Moschou, N. Vourdas, V. Tsouti, G. Kokkoris, G. Tsekenis, I. Zergioti, A. Tserepi, S. Chatzandroulis
    5th International Conference on Micro-Nanoelectronics, Nanotechnologies and MEMS, 7-10 October 2012, Kokkini Hani, Heraklion, Greece
14. *Autonomous, plasma-nanotextured, smart microfluidics, and Lab-on-Chip systems for chemical and biological analysis* (oral),
    Evangelos Gogolides, Katerina Tsougeni, Kosmas Ellinas, Angeliki Tserepi, Panagiota Petrou, and Sotirios Kakabakos
    Micro and Nano 2012

D3. Nano-Devices for Energy

15. *High aspect ratio, plasma etched silicon nanowires for photovoltaic application: Fabrication and characterization* (Invited talk),
    A. Smyrnakis, A. Zeniou, E. Almpanis, N. Papanikolaou, P. Dimitrakis, E. Gogolides,
    XI International Conference on Nanostructured Materials (NANO 2012) August 26-31, 2012, Rhodes, Greece

Seminars – Invited talks

1. *Morphological characterization of nanostructures through the analysis of SEM images* (invited talk),
   V. Constantoudis, V.K. Murugesan Kuppuswamy, N. Karasmani, G. Giannakopoulos, E. Gogolides
   9th International Conference on Nanosciences & Nanotechnologies (NN) July 3-6, 2012, Thessaloniki, Greece
2. *High aspect ratio, plasma etched silicon nanowires for photovoltaic application: Fabrication and characterization* (Invited talk),
   A. Smyrnakis, A. Zeniou, E. Almpanis, N. Papanikolaou, P. Dimitrakis, E. Gogolides, XI International Conference on Nanostructured Materials (NANO 2012) August 26-31, 2012, Rhodes, Greece
3. *Morphological characterization of nanostructures through the analysis of SEM and AFM images* (invited talk),
   V. Constantoudis, V.K. Murugesan Kuppuswamy, N. Karasmani, G. Giannakopoulos, E. Gogolides
   38th International Micro & Nano Engineering Conference (MNE), September 16-20, 2012, Toulouse, France
4. *Autonomous, plasma Nanotextured smart microfluidics, and Lab on a Chip systems for chemical and biological analysis* (invited talk),
   E. Gogolides, K. Tsougeni, K. Ellinas, A. Tserepi, P. Petrou, S. Kakabakos
   5th International Conference on Micro-Nanoelectronics, Nanotechnologies and MEMS, 7-10 October 2012, Kokkini Hani, Heraklion, Greece
5. *Micro & Nanofluidics: Technology and Applications,*
   A.Tserepi
   Summer School “Nanomaterials and Devices”, University of Patras, July 12, 2012, Patras

Conference Participation

- 26th SPIG 2012
- SPIE 2012 - The International Society for Optical Engineering
- 13th International Conference on Plasma Surface Engineering (PSE 2012)
- EMRS 2012 Meeting
- 16th Int. Conference on Miniaturized Systems for Chemistry and Life Sciences (μTAS)
- 3rd European Microfluidics Conference
- Plasma Etch and Strip in Microelectronics (PESM 2012)
- XI International Conference on Nanostructured Materials (NANO 2012)
- 38th International Micro & Nano Engineering Conference (MNE 2012)
- European Congress on computational methods in applied science and engineering (ECCOMAS 2012)
- 5th International Conference on Micro-Nanoelectronics, Nanotechnologies and MEMS
- Micro and Nano 2012
- XI International Conference on Nanostructured Materials (NANO 2012)
- 9th International Conference on Nanosciences & Nanotechnologies (NN)

Masters Dissertations completed in 2012

1. *Mathematical modeling of a continuous flow microfluidic device for DNA amplification by Polymerase Chain Reaction,*
   Elias Kouris
   MSc Thesis held at IMEL/NCSR Demokritos (Supervisors: G. Kokkoris, A. Tserepi),
   Defended at the National and Kapodistrian University of Athens, Physics Department 2012
2. *Nanopillars and vertical silicon nanowires fabrication using silicon plasma etching processes in room temperature,*
   Angelos Zeniou
   MSc Thesis held at IMEL/NCSR Demokritos (Supervisor: E. Gogolides)
   Defended at the National and Kapodistrian University of Athens, Dept. of Informatics and Telecommunications 2012
3. *Analysis of Rough Surfaces with Network Theory,*
   Nikoletta Karasmani, MSc Thesis held at IMEL/NCSR Demokritos (Supervisor: V. Constantoudis), Defended at National Technical University of Athens, School of Applied Mathematical and Physical Sciences 2012

Doctoral Dissertations completed in 2012

Contact edge roughness in EUV lithography: Metrology and process evaluation,
Vijayakumar Murugesan Kuppuswamy

National Technical University of Athens, School of Chemical Engineering, Athens, Thesis Research Supervisor at NCSR Demokritos: Dr. E. Gogolides, Dr V. Constantoudis, Thesis Supervisor at NTUA: Prof. A. Boudouvis

Teaching and Training Activities

- *Microelectronics and Microsystems fabrication processes,*
  (E. Gogolides, D. Davazoglou, A. Nassiopoulou), Postgraduate Programs on Microsystems and Nanodevices of the National Technical University of Athens and Micro and Nano Electronics of the National and Kapodistrian Univ. of Athens
- *Plasma Processing for Micro and Nano Fabrication,*
  (E. Gogolides, G. Kokkoris, V. Constantoudis, A. Tserepi), Postgraduate Program on Microelectronics of the National and Kapodistrian Univ. of Athens
- *Microfluidic systems,*
  (D. Mathioulakis, I. Anagnostopoulos, A. Tserepi, G. Kokkoris), Postgraduate Program on Microsystems and Nanodevices of the National Technical University of Athens
- *SimulationofMicroandNano-Patterning*,
  (E. Gogolides, G. Kokkoris, V. Constantoudis, A. Tserepi), Postgraduate Program on Mathematical Modelling in Modern Technologies and Financial Engineering of the NationalTechnicalUniversity of Athens
- *Fractal geometry and its applications in microelectronics,*
  (V. Constantoudis), Demokritos Summer School, 05-16 July 2010
- *Process and device simulation,*
  (G. Kokkoris), Postgraduate Program on Microelectronics of the National and Kapodistrian University of Athens
- *Plasma etching for microelectronics, MEMS, Lab-on-Chip fabrication and nanotechnology,*
  Short Course, E. Gogolides, 18th International Colloquium on Plasma Processes (CIP 2011), 4-8 July 2011, Nantes, France